

1 Hydroxyl radicals from secondary organic aerosol decomposition in water

2

3 Haijie Tong¹, Andrea M. Arangio¹, Pascale S. J. Lakey¹, Thomas Berkemeier¹, Fobang Liu¹,
4 Christopher J. Kampf^{1,2}, William H. Brune³, Ulrich Pöschl¹ & Manabu Shiraiwa^{1,*}

5 ¹ Multiphase Chemistry Department, Max Planck Institute for Chemistry, Mainz, Germany

6 ² Institute for Inorganic and Analytical Chemistry, Johannes Gutenberg University Mainz, Mainz,
7 Germany

8 ³ Department of Meteorology, Pennsylvania State University, University Park, PA 16802, USA

9

10 * Correspondence to M. Shiraiwa (m.shiraiwa@mpic.de)

11

12 **Abstract.**

13 We found that ambient and laboratory-generated secondary organic aerosols (SOA) form
14 substantial amounts of OH radicals upon interaction with liquid water, which can be explained by the
15 decomposition of organic hydroperoxides. The molar OH yield from SOA formed by ozonolysis of
16 terpenes (α -pinene, β -pinene, limonene) is $\sim 0.1\%$ upon extraction with pure water and increases to
17 $\sim 1.5\%$ in the presence of Fe^{2+} ions due to Fenton-like reactions. Upon extraction of SOA samples
18 from OH photooxidation of isoprene, we also detected OH yields of around $\sim 0.1\%$, which increases
19 upon addition of Fe^{2+} . Our findings imply that the chemical reactivity and aging of SOA particles is
20 strongly enhanced upon interaction with water and iron. In cloud droplets under dark conditions, SOA
21 decomposition can compete with the classical H_2O_2 Fenton reaction as the source of OH radicals.
22 Also in the human respiratory tract, the inhalation and deposition of SOA particles may lead to a
23 substantial release of OH radicals, which may contribute to oxidative stress and play an important role
24 in the adverse health effects of atmospheric aerosols.

25

26 **1. Introduction**

27 Secondary organic aerosols (SOA) account for a major fraction of fine air particulate matter
28 and have a strong influence on climate and public health (Jimenez et al., 2009; Pöschl et al., 2010;
29 Huang et al., 2014). Formation of SOA is triggered by oxidation of volatile organic compounds
30 followed by condensation of semi-volatile oxidation products (Hallquist et al., 2009; Donahue et al.,
31 2012). Recently, it has been shown that extremely low volatility organic compounds (ELVOC)
32 contribute significantly to SOA growth (Ehn et al., 2014; Jokinen et al., 2015; Mentel et al., 2015).

33 Particle phase chemistry and cloud processing are also efficient pathways for SOA formation
34 and aging (Kalberer et al., 2004; Herrmann et al., 2005; Ervens et al., 2011; Shiraiwa et al., 2013).
35 Evolution of SOA is one of the largest uncertainties in the current understanding of air quality,
36 climate and public health (Kanakidou et al., 2005; Solomon, 2007). With regard to SOA health effects,
37 substantial amounts of reactive oxygen species including organic radicals are detected in ambient and
38 laboratory-generated SOA (Venkatachari and Hopke, 2008; Chen and Hopke, 2010; Chen et al., 2010;
39 Fuller et al., 2014). Despite intensive research, multiphase chemical reactions of SOA in the
40 atmosphere and upon interaction with the human respiratory tract are not well understood (Pöschl and
41 Shiraiwa, 2015).

42 OH radicals in atmospheric droplets originate from the uptake of gaseous OH radicals (Jacob,
43 1986; Arakaki et al., 2013) as well as photolysis of ozone (Anglada et al., 2014). A recent study has
44 shown that SOA can form OH radicals in the aqueous phase under light conditions (Badali et al.,
45 2015). Under dark conditions, Fenton reactions between H₂O₂ and iron ions have been regarded as the
46 main source of OH radicals so far (Herrmann et al., 2005). In this study, we found that OH radicals
47 are formed by decomposition of SOA upon interactions of water and iron ions under dark conditions.

48

49 **2. Methods**

50 **2.1 SOA formation and particle collection**

51 Fig. 1 shows the experimental setup for generation of secondary organic aerosols (SOA). O₃
52 was used as oxidant for oxidation of α -pinene, β -pinene, limonene, and OH radicals were used for
53 naphthalene. O₃ was generated via synthetic air (Westfalen AG, 1.8-2.1 L/min) passing through a 185

54 nm UV light (O_3 generator, L.O.T.-Oriol GmbH & Co. KG). The typical ozone concentrations were
55 600 ppb for α -pinene, β -pinene and limonene, and 1200 ppb for naphthalene. 1 mL of α -pinene (98%,
56 Sigma Aldrich), β -pinene (99%, Sigma Aldrich) or limonene (99%, Sigma Aldrich) was kept in a 1.5
57 mL amber glass vial (VWR International GmbH), and 5-10 g of naphthalene crystals (99.6%, Alfa
58 Aesar GmbH & Co. KG) were put in a 100 mL glass bottle (DURAN Group GmbH) as SOA
59 precursor sources. 1 bar and 50-150 ccm/min N_2 (99.999%, Westfalen AG) flow was passed through
60 these sources and the evaporated VOC vapours were introduced into a 7 L quartz flow tube reactor for
61 gas-phase oxidation reaction with O_3 or OH radicals with a reaction time of ~ 3 minutes. SOA by α -
62 pinene, β -pinene, and limonene were generated under dark and dry conditions. The flow tube reactor
63 is surrounded by 4 UV-lights (wavelength of 254 nm, LightTech Lamp Technology Ltd.), which were
64 turned on to generate OH radicals by photolysis of ozone and water vapour. The relative humidity in
65 the flow tube was 30% for generating naphthalene SOA, and other experiments were conducted under
66 dry conditions. Isoprene SOA was produced in a potential aerosol mass (PAM) chamber through the
67 reaction of gas phase OH radicals and isoprene. The detailed information about this chamber has been
68 described elsewhere (Kang et al., 2007; Lambe et al., 2011) and the SOA generated by the PAM
69 chamber have been shown to be similar to SOA generated in large environmental chambers (Bruns et
70 al., 2015; Lambe et al., 2015) and the atmosphere (Ortega et al., 2015) in terms of oxidation state and
71 chemical composition. Briefly the isoprene vapour was taken into the chamber by N_2 gas with an
72 estimated concentration of tens of ppm. Ozone concentration in the PAM was 6-15 ppm and relative
73 humidity was 30-40%.

74 Number concentration and size distribution of the generated SOA particles were characterized
75 using the Scanning Mobility Particle Sizer (SMPS, GRIMM Aerosol Technik GmbH & Co. KG). The
76 typical size of the SOA ranged from 50 to 400 nm. The median diameters of the mass size distribution
77 were 100 – 200 nm. MnO_2 (copper mesh covered with MnO_2 from ANSYCO Analytische Systeme
78 und Componenten GmbH fixed in Gelman filter) and charcoal (4-8 mesh, Sigma Aldrich) denuders
79 were used to remove unreacted O_3 before the collection of SOA particles on a filter. SOA was
80 collected on 47 mm Omnipore Teflon filters (100 nm pore size, Merck Chemicals GmbH). The
81 concentration of O_3 was monitored after an ozone denuder with an ozone analyser (typically 0-20 ppb,

82 model 49j, Thermo Fisher Scientific Inc.). 2 silica gel (2-4 mm, Carl Roth GmbH + Co. KG) denuders
83 were used to dry the naphthalene SOA before collection.

84 Blank tests confirmed that no radicals were produced without SOA particles on a filter.
85 Condensation of water vapour on a filter during SOA collection was negligible. A Teflon filter with
86 particle loading was weighed using a XSE105DU balance with accuracy of $\pm 20 \mu\text{g}$. It was then
87 immersed into a 0.5-1 mL 10 mM BMPO water solution and stirred with a vortex shaker (Heidolph
88 Reax 1) for 2-7 minutes for particle extraction. A typical extraction efficiency of $>70\%$ in weight can
89 be obtained with 7 min extraction time. After extraction, the filter was dried under 2-3 bar N_2 for ~ 10
90 minutes and the filter was weighed. The weight difference was regarded as the weight of extracted
91 particles. The final SOA concentration depends on the extraction time and the average molar mass of
92 SOA was assumed to be 200 g mol^{-1} in calculating SOA concentrations. The pH of SOA solutions
93 was in the range of 4.8 - 6.4.

94 The Micro-Orifice Uniform Deposition Impactors (MOUDI, 110-R mode, MSP Corporation)
95 was used for collection of ambient particles on the roof of the Max Planck Institute for Chemistry
96 (Mainz, Germany) in 24 hour time resolution with a flow rate of 30 L/min from 17:30 PM 4th June
97 2015 to 17:30 PM 5th June 2015, and from 17:30 PM 7th June 2015 to 17:30 PM 8th June 2015.
98 Particles within the diameter range of 180 – 320 nm, which is the size range dominated by organic
99 aerosols in Mainz (Faber et al., 2013), were used for further analysis. The mass loading of these two
100 samples on filters were ~ 70 and $80 \mu\text{g}$, respectively. 47 mm diameter Teflon filters (100 nm pore size,
101 Merck Chemicals GmbH) were used to collect the roof particles. Filters were cleaned with pure
102 ethanol and ultra-pure water and dried by nitrogen gas before sampling and weighing. The extraction
103 procedure is the same as that for laboratory SOA, and the field particle extracts were concentrated
104 with a N_2 flux to obtain high signal to noise ratio spectra. Concentration of field particles in water
105 extracts for EPR measurements were $\sim 0.3 \text{ g L}^{-1}$, which is in the same order of magnitude as extracts
106 of laboratory-generated SOA.

107

108 **2.2 CW-EPR**

109 Continuous Wave Electron Paramagnetic Resonance (CW-EPR) spectroscopy (EMXplus-
110 10/12, Bruker, Germany) was applied for detection of radicals. 15-30 μL sample solutions were kept
111 in a 50 μL capacity micropipette and inserted into a highly sensitive cavity (E4119001 HS-W1) for
112 analysis. The set of EPR parameters used for this study was as follows: a modulation frequency of
113 100 kHz; a modulation amplitude of 0.6 or 1; microwave power of 2.149 mW (20 dB) or 21.17 mW
114 (10 dB); a receiver gain of 40 dB; a time constant of 0.01 ms, and a magnetic field scan of 100 G.
115 After the SOA extraction, the samples were immediately analysed by an EPR.

116 The spin trap 5-tert-Butoxycarbonyl-5-methyl-1-pyrroline-N-oxide (BMPO, high purity, Enzo
117 Life Sciences GmbH) was used as a trapping agent of OH radicals. Compared to other spin trapping
118 agents such as 5, 5-dimethyl-1-pyrroline *N*-oxide (DMPO), BMPO has the following advantages: high
119 purity and stability in the crystalline phase; highly distinguishable EPR spectra for different structure
120 of the trapped radicals; and spectra with high signal to noise ratio. Buffer solutions are often used in
121 the spin trapping technique, but were not used in this study to avoid changing the real acidity
122 environment of SOA solutions. A BMPO concentration of 10 mM was used. No significant difference
123 was observed among 10, 20, 30, 40, and 50 mM BMPO solutions, confirming that a BMPO
124 concentration of 10 mM is sufficient to achieve the maximum trapping efficiency. The influence of
125 the BMPO concentration on the aqueous phase OH radical trapping efficiency for β -pinene SOA was
126 investigated as shown in Fig. S3. Further blank tests confirmed that H_2O_2 (30%, Sigma Aldrich), Fe^{2+} ,
127 and Fe^{3+} ($\text{Fe}_2\text{O}_3 \cdot x\text{H}_2\text{O}$, 97%, Sigma Aldrich) do not induce OH radical formation when each of
128 them is mixed with BMPO in water (Fig. S4).

129 The spin counting method was applied for quantification of OH radicals using the embedded
130 subroutine of the Bruker Xenon software (Weber, 2012). For better quantification of detected radicals,
131 the spin fitting method (Bruker Xenon software, chapter 13 (Weber, 2012)) was used to increase the
132 signal to noise ratio especially for low radical concentrations. The required parameters are hyperfine
133 splitting parameters for OH radicals, which were taken from Zhao et al. (2001). Spectral simulations
134 for radical adducts were carried out using the Matlab-based computational package Easyspin (Stoll
135 and Schweiger, 2006). A global optimization (genetic algorithm) was conducted to obtain parameters
136 for simulating the EPR spectrum. The parameter set was further optimized using the particle swarm

137 method within the Easyspin program. The function 'garlic' for cw EPR spectra in isotropic and fast
138 motion regimes were chosen for simulation. The hyperfine splitting constants for simulation were
139 taken from the previous work (Zhu et al., 2009).

140

141 **2.3 LC-MS/MS**

142 The SOA extracts mixed with spin trapping agent BMPO were also analysed with a
143 nanoHPLC-chip-MS/MS system (Agilent), which consists of a nano pump (G2226A) with 4-channel
144 micro-vacuum degasser (G1379B), a microfluidic chip cube with electrospray ionization (ESI) source
145 (G4240-62010) interfaced to a Q-TOF mass spectrometer (6540; nominal mass resolution 30000 at a
146 scan rate of 5 s^{-1}), a capillary pump (G1376A) with degasser (G1379B), and an auto-sampler with
147 thermostat (G1377A). All modules were controlled by Mass Hunter software (Rev. B.05.01, Agilent).
148 Eluents used were: 3% (v/v) acetone nitrile (Chromasolve, Sigma, Seelze, Germany) in water/formic
149 acid (0.1% v/v, Chromasolv, Sigma, Seelze, Germany) (Eluent A), and 3% water/formic acid (0.1%
150 v/v) in acetone nitrile (Eluent B). The flow rate was 400 nL min^{-1} with a gradient program that
151 starting with 3% B for 3 min followed by a 36 min step that raised eluent B to 60%. Further, the
152 eluent B was increased to 80% at 40 min, and returning to initial conditions within 0.1 min, followed
153 by column re-equilibration for 9.9 min before the next run. The ESI-Q-TOF instrument was operated
154 in the positive ionization mode (ESI+) with an ionization voltage of 1900 V. Fragmentation of
155 protonated ions was conducted using the auto MS/MS mode. Spectra were recorded over the mass
156 range of m/z 100-3000. Data analysis was performed using the Qualitative Data Analysis software
157 (Rev. B. 06.00, Agilent).

158

159 **2.4 Kinetic Modelling**

160 The chemical reactions used to describe the BMPO/SOA/ Fe^{2+} / H_2O system, including Fenton-
161 like reactions, are listed along with their rate coefficients in Table S1. From this set of 25 reactions, 16
162 were optimized using the MCGA method and parameter ranges are given in the Table S1 to illustrate
163 the uncertainty arising from global optimization. For all other parameters reference values were taken
164 from literature, which remained fixed during optimization. Kinetic rate coefficients of a large set of

165 chemical reactions were determined using a uniformly sampled Monte Carlo search seeding a genetic
166 algorithm (MCGA method (Berkemeier et al., 2013; Arangio et al., 2015)) as the global optimization
167 method. This algorithm optimizes a kinetic model to experimental data and avoids to getting trapped
168 in local minima during the optimization process. In the kinetic model, ROOH represents all organic
169 hydroperoxides without resolving individual structures. This is a simplification, which is necessary
170 for the kinetic modelling but seems to return consistent results.

171

172 **3. Results and Discussion**

173 Figure 2 indicates that EPR spectra of laboratory generated SOA by α -pinene (A), β -pinene
174 (B), limonene (C), and isoprene (D) SOA were composed of four major peaks, whereas naphthalene
175 SOA (E) exhibited no significant signals. These four peaks were also found for field samples (F) and
176 became more prominent in the presence of Fe^{2+} (G). In addition, the same splitting was also observed
177 in a solution of tert-Butyl hydroperoxide (H). Four-lines signals generated by hyperfine splittings are
178 characteristic for BMPO-trapped OH radicals in water solution, as shown in the spectrum (I) for
179 solutions of H_2O_2 and Fe^{2+} generating OH via the Fenton reaction ($\text{Fe}^{2+} + \text{H}_2\text{O}_2 \rightarrow \text{Fe}^{3+} + \text{OH}^- + \cdot\text{OH}$)
180 (Zhao et al., 2001).

181 Figure 3 shows LC-MS chromatograms of the BMPO-OH adduct (m/z 216.121) for aqueous
182 BMPO solutions (black line) and for BMPO in aqueous β -pinene SOA extract (red line). A strong
183 peak is observed at a retention time of 11.6 minutes for BMPO in aqueous β -pinene SOA extract, but
184 not for the aqueous BMPO solution, which served as a blank. Confirmation of the BMPO structure for
185 m/z 216.121 was achieved by comparing MS^2 spectra of $[\text{BMPO}+\text{H}^+]^+$ (m/z 200.126) from the
186 aqueous standard and m/z 216.121. In both cases the loss of a characteristic fragment with a mass of
187 56.062 Da is observed (panel c and f), which corresponds to the loss of C_4H_8 from the t-
188 butoxycarbonyl function of BMPO. Above LC-MS/MS analysis confirms the presence of OH radicals
189 in β -pinene SOA extracts observed by EPR shown in Fig. 2.

190 The EPR and LC-MS/MS observations provide strong evidence that OH radicals are
191 generated in water extracts of SOA by α -pinene, β -pinene, limonene, and isoprene as well as field fine

192 particles, which can be enhanced by Fe^{2+} . Note that additional hyperfine splitting are observed for
193 monoterpene and isoprene SOA and especially for field samples, indicating the presence of organic
194 radicals. Figure 4a shows that the amount of OH radicals trapped by BMPO increases as the SOA
195 concentration increases in the aqueous phase. The OH yield from β -pinene SOA is the highest
196 generating $\sim 1.5 \mu\text{M}$ of OH radicals at 1.5 mM SOA concentration, followed by α -pinene, isoprene,
197 and limonene SOA. Naphthalene SOA has a negligible yield of OH radicals.

198 For assessment of potential interferences from trace amounts of impurities such as transition
199 metals in water, the OH yield was also measured in water with three different purity grades: Milli-Q
200 water (18.2 M, Thermo Scientific™ Barnstead™ GenPure™ xCAD Plus ultrapure water system),
201 TraceSELECT® Ultra ACS reagent water (Sigma Aldrich), and Savillex water (DST-1000 Acid
202 Purification System), which results in excellent agreement (Fig. 5) confirming that OH radicals can be
203 formed in the absence of transition metals.

204 Ambient particulate matter is often associated with iron ions, which play an important role in
205 aerosol chemistry via Fenton-like reactions (Deguillaume et al., 2005). To investigate the effects of
206 transition metals on OH formation by SOA, different concentrations of Fe^{2+} were added in SOA water
207 extracts. Fig. 4b-d show the OH formation efficiency (molar concentration ratio of OH and SOA:
208 $[\text{BMPO-OH}]/[\text{SOA}]$, in %) of β -pinene, α -pinene and limonene SOA as a function of molar
209 concentration ratio of FeSO_4 to SOA ($[\text{Fe}^{2+}]/[\text{SOA}]$). The OH formation efficiency reaches maximum
210 values of 1.5% for β -pinene SOA, 1.1% for α -pinene SOA, and 0.5% for limonene. Different
211 behaviours in OH formation efficiency of limonene compared to α -pinene and β -pinene may be
212 induced by different organic hydroperoxide concentrations and different R subgroup structure of
213 ROOH. This order is the same as the order of the relative contribution of organic peroxides in these
214 types of SOA (Docherty et al., 2005). For isoprene SOA, the first results of ongoing experiments
215 indicate a significant increase of OH yield with increasing Fe^{2+} concentrations. The EPR spectra of
216 the isoprene SOA show a dependence on the oxidant concentration level in the PAM chamber. The
217 more complex behaviour of the isoprene SOA from OH photooxidation is under investigation and will
218 be presented in a follow-up study.

219 The observed formation of OH radicals is most likely due to hydrolysis and thermal
220 decomposition of organic hydroperoxides (ROOH), which account for the predominant fraction of
221 terpene SOA (Docherty et al., 2005; Epstein et al., 2014) as well as in rain water (Hellpointner and
222 Gäb, 1989), but have little contribution for naphthalene SOA (Kautzman et al., 2010). ROOH are
223 formed via multigenerational gas-phase oxidation and autoxidation, introducing multiple hydroperoxy
224 functional groups forming extremely low volatility organic compounds (Crouse et al., 2013; Ehn et
225 al., 2014). Due to the low binding energy of the O-O bond induced by the electron-donating R group,
226 ROOH are well-known to undergo thermal homolytic cleavage ($\text{ROOH} \rightarrow \text{RO}^\bullet + \bullet\text{OH}$, (Nam et al.,
227 2000)). In the presence of Fe^{2+} , it has been reported that decomposition of ROOH can be enhanced
228 mainly via Fenton-like reactions leading to heterolytic cleavage of the O-O bond in the following two
229 ways depending on the pH and reaction environments: $\text{ROOH} + \text{Fe}^{2+} \rightarrow \text{RO}^\bullet + \text{OH}^- + \text{Fe}^{3+}$ or ROOH
230 $+ \text{Fe}^{2+} \rightarrow \text{RO}^- + \bullet\text{OH} + \text{Fe}^{3+}$ (Goldstein and Meyerstein, 1999; Deguillaume et al., 2005). Note that
231 homolytic cleavage can be catalyzed by iron ions (Foster and Caradonna, 2003). The formed alkoxy
232 radicals (RO^\bullet) were trapped by BMPO and found to increase as the Fe^{2+} concentration increases (Fig.
233 6). The formation of organic radicals in α -pinene and limonene SOA has been also detected in the
234 previous studies (Pavlovic and Hopke, 2010; Chen et al., 2011). As shown in Fig. 4, the chemical box
235 model including the above three ROOH decomposition pathways reproduces experimental data very
236 well, strongly suggesting that the source of OH radicals is decomposition of ROOH. The decrease of
237 OH radical production with increasing Fe^{2+} concentration is supposedly induced by reaction of the
238 BMPO-OH adduct with Fe^{2+} (Yamazaki and Piette, 1990) (see also SI).

239 It has been suggested that hydrogen peroxide (H_2O_2) can be generated from α - and β -pinene
240 SOA in water, but the mass yield of H_2O_2 is $\sim 0.2\%$ (Wang et al., 2011). In the presence of Fe^{2+} , H_2O_2
241 can yield OH radicals via the Fenton reaction and the formation efficiency of BMPO-OH adduct by
242 mixtures of H_2O_2 with Fe^{2+} was measured to be $\sim 0.6\%$ (Fig. S2). Thus, the potential contribution of
243 generated H_2O_2 to OH yields in β - and α -pinene SOA extracts is much lower than the observed OH
244 radicals. Moreover, the OH yield was not affected, even if β -pinene SOA was dried under a N_2 flow

245 before the water extraction to evaporate particle-phase H₂O₂. Hence it is clear that the H₂O₂ in SOA
246 should not be the dominant source of OH radicals observed in this study.

247

248 **4. Implications**

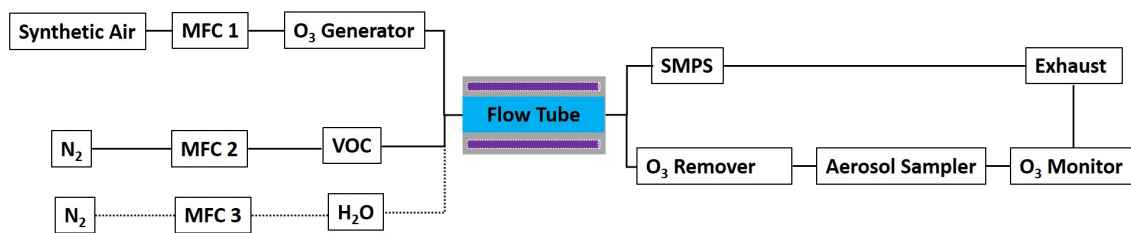
249 The implications of this finding are illustrated in Figs. 7 and 8. The orange area in Fig. 7a
250 shows OH production rate by Fenton reactions between Fe²⁺ and H₂O₂ forming OH radicals as a
251 function of H₂O₂ concentration with typical dissolved iron concentrations in cloud droplets of 0.1 –
252 2.5 μM (Deguillaume et al., 2005). The green area shows the OH production rate by SOA
253 decomposition in cloud or fog droplets, which ranges from ~0.01 – 100 nM s⁻¹ depending on SOA
254 precursors and the Fe²⁺ and SOA concentrations (see supplement). It clearly shows that SOA
255 decomposition is comparably important to the Fenton reaction in most conditions and SOA can be the
256 main source of OH radicals at low concentrations of H₂O₂ and Fe²⁺. Water-soluble gases such as
257 aldehydes taken up by deliquesced particles may undergo reactions in the presence of OH radicals to
258 form low volatility products, including organic acids, peroxides, peroxyhemiacetals and oligomers
259 (Lim et al., 2010; Ervens et al., 2011; Liu et al., 2012; Ervens, 2015; Lim and Turpin, 2015; McNeill,
260 2015). Thus, the formed OH radicals would promote chemical aging of SOA especially in the
261 presence of iron ions (e.g., SOA coated mineral dust particles) (Chu et al., 2014) and may also induce
262 aqueous-phase oxidation of sulfur dioxide forming sulfuric acid (Harris et al., 2013).

263 Recent studies have shown that OH radicals can trigger autoxidation reactions in the gas
264 phase, generating highly oxidized and extremely low volatility compounds (Crouse et al., 2013; Ehn
265 et al., 2014). In addition, it has been shown that some radicals can be long-lived in the condensed
266 phase (Shiraiwa et al., 2011b; Gehling and Dellinger, 2013) by interacting with transition metals
267 (Truong et al., 2010). We hypothesize that OH radicals formed from SOA decomposition could also
268 trigger autoxidation in the condensed phase. Such a self-amplification cycle of SOA formation and
269 aging may be relevant for example in the Amazon, where cloud and fog processing are important
270 pathways forming a high fraction of SOA with high O:C ratio, resulting in an enhancement of cloud
271 condensation nuclei activity of particles (Pöschl et al., 2010; Pöhlker et al., 2012). Organic peroxides
272 are often used as the agent of the vulcanization processes to initiate the radical polymerization by

273 forming free radicals, which abstract hydrogen atoms from the elastomer molecules converting them
274 into radicals that undergo oligomerization to form elastic polymer or rubber. Similar processes might
275 also occur in SOA particles (“SOA vulcanization”), which may contribute to formation of dimers and
276 oligomers observed in SOA particles (Kalberer et al., 2004) possibly leading to the occurrence of an
277 amorphous solid state (Virtanen et al., 2010; Koop et al., 2011; Shiraiwa et al., 2011a; Renbaum-
278 Wolff et al., 2013; Kidd et al., 2014).

279 In indoor air, terpenes are commonly found at higher concentrations than in the ambient air
280 due to their widespread use as solvents and odorants in cleaning products and air fresheners (Weschler,
281 2011). Depending on precursor concentrations, the SOA concentration in indoor air can reach up to 30
282 $\mu\text{g m}^{-3}$ with the highest contribution from limonene SOA (Waring, 2014). To evaluate potential
283 adverse health effects by SOA deposition into the lungs, we estimated the OH production rate by SOA
284 within the lung lining fluid (LLF) as a function of ambient SOA concentration considering breathing
285 and deposition rates (see supplement) (Fig. 7b). The pH of lung lining fluid for healthy people is
286 about 7.4. Our recent experiments have shown that the formation of OH radicals was increased by
287 ~20% at a pH of 7.4 in a phosphate-buffered saline solution. Thus, the OH production rate by SOA
288 decomposition shown in Fig. 7b may represent the lower limit. We intend to investigate pH effects on
289 OH formation in detail in follow-up studies.

290 Fig. 7b also shows the OH production rate by the Fenton reaction with typical iron
291 (Gutteridge et al., 1996) and H_2O_2 concentrations in the LLF (Corradi et al., 2008). Patients with
292 respiratory diseases are reported to have high H_2O_2 concentrations in the bronchoalveolar lavage
293 (Corradi et al., 2008) (as shown in shaded purple area) and the Fenton reaction may be the main
294 source of OH radicals for such patients. However, for healthy people with low H_2O_2 and Fe^{2+}
295 concentrations, SOA decomposition can be more important than the Fenton process under high
296 ambient or indoor SOA concentrations. Excess concentrations of reactive oxygen species including
297 hydrogen peroxide, OH radicals (and potentially also organic radicals) are shown to cause oxidative
298 stress to human lung fibroblasts, alveolar cells and tissues (Pöschl and Shiraiwa, 2015). Thus, in
299 polluted indoor or urban megacities with high SOA concentration such as in Beijing, SOA particles
300 may play a critical role in adverse aerosol health effects.



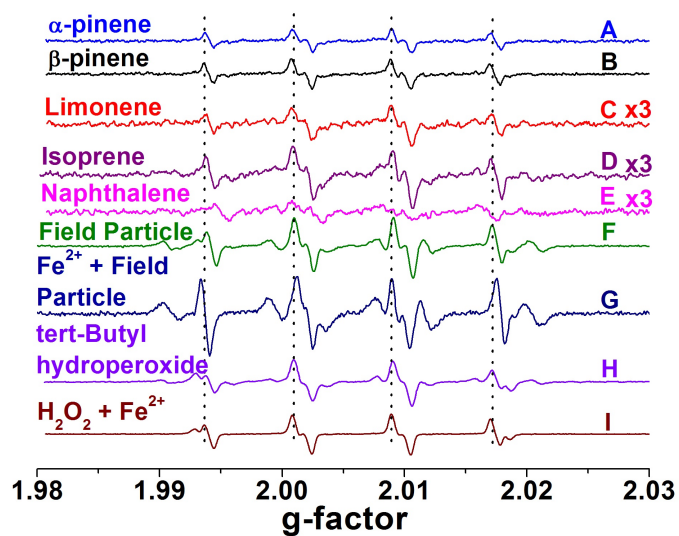
301

302

303 **Figure 1. Schematics of the experimental setup for generation and collection of SOA particles.**

304

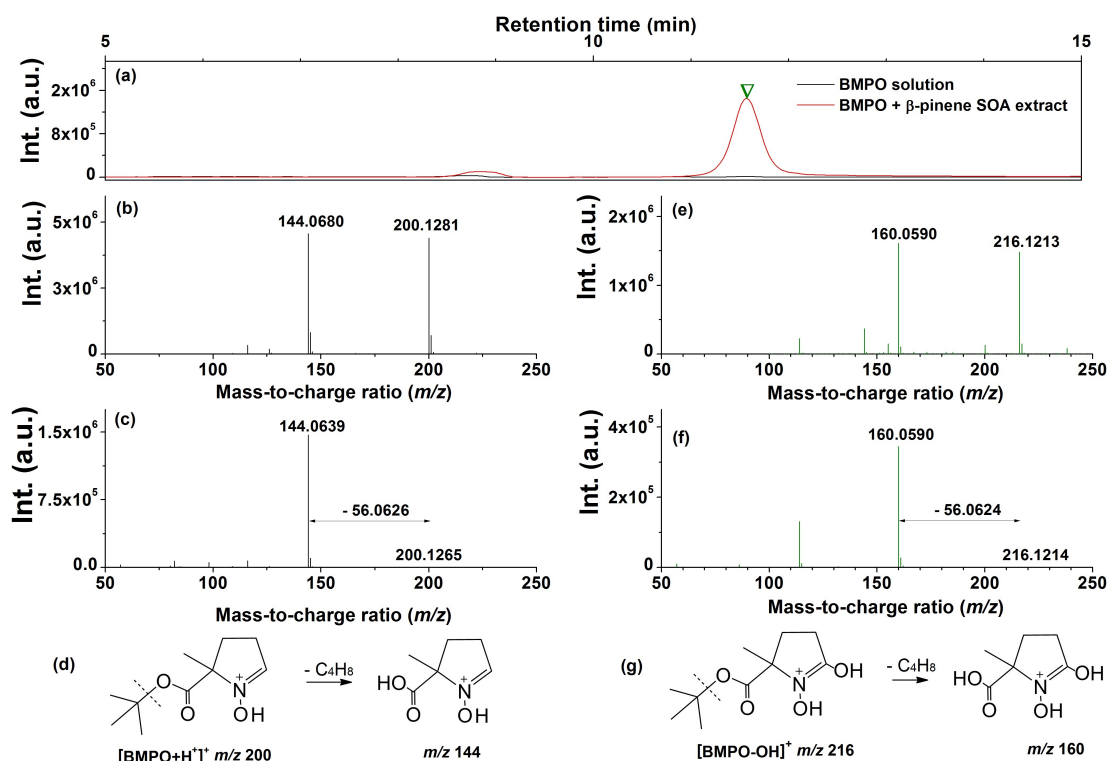
305



306

307 **Figure 2. EPR spectra of sample solutions mixed with the spin trapping agent BMPO:** (A) α -
308 pinene SOA, (B) β -pinene SOA, (C) limonene SOA, (D) isoprene SOA, (E) naphthalene SOA, (F)
309 180 - 320 nm size field particles, (G) 180 - 320 nm size field particles mixed with Fe^{2+} , (H) tert-Butyl
310 hydroperoxide solution, and (I) H_2O_2 solution with Fe^{2+} . The four peaks (dotted lines) are
311 characteristic for BMPO-OH adducts.

312

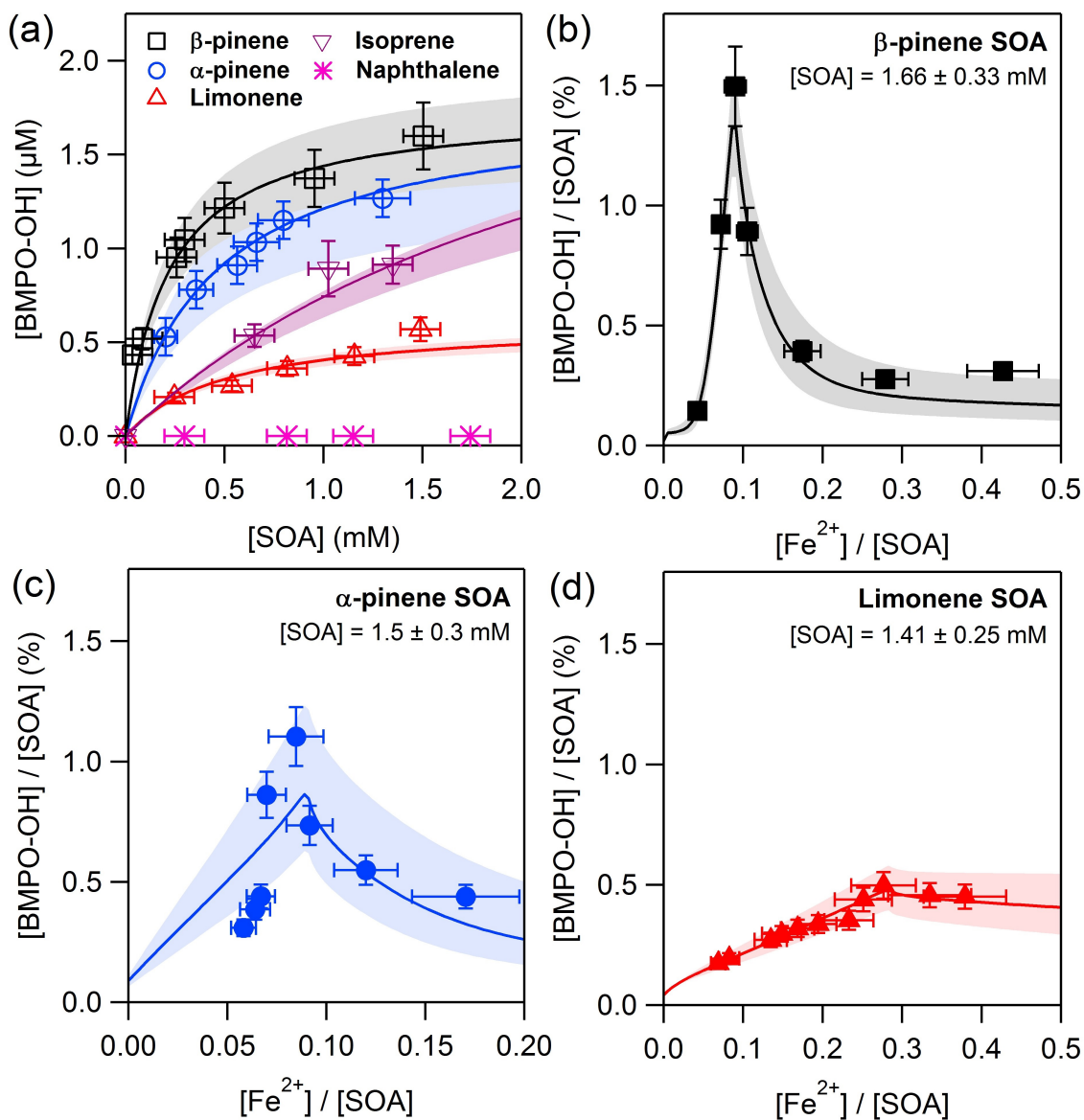


313

314 **Figure 3. LC-MS/MS analysis.** (a) LC-MS chromatogram of aqueous BMPO solution (black line)
 315 and BMPO mixed with β -pinene SOA water extracts (red line). The downward triangle indicates the
 316 retention time of m/z 216 (BMPO-OH). (b) MS spectrum of $[\text{BMPO}+\text{H}]^+$ with nominal m/z 200. (c)
 317 MS^2 spectrum of m/z 200, with the characteristic fragment ion m/z 144.0639 ($[\text{BMPO}+\text{H}]^+ - m/z$
 318 56.0626). (d) Proposed fragmentation pathway for m/z 200. The most abundant fragment ion present
 319 in (c) corresponds to the loss of C_4H_8 from $[\text{BMPO}+\text{H}]^+$. (e) MS spectrum of $[\text{BMPO}-\text{OH}]^+$ with m/z
 320 216. (f) The MS^2 spectrum of m/z 216, with the characteristic fragment ion m/z 160.0590 ($[\text{BMPO}-$
 321 $\text{OH}]^+ - m/z$ 56.0624). (g) Proposed fragmentation pathway for m/z 216. The observed loss of C_4H_8 is
 322 characteristic for the fragmentation of the *t*-butoxycarbonyl function of BMPO.

323

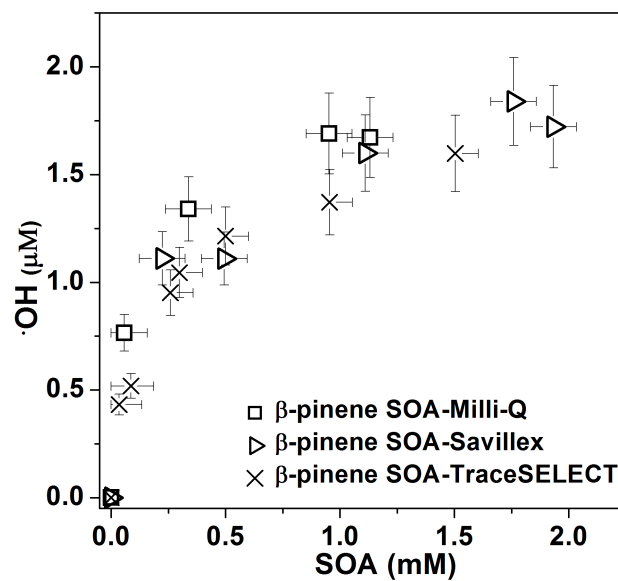
324



326

327 **Figure 4. OH formation efficiency by SOA.** (a) Concentrations of OH radicals formed in water
 328 extracts of SOA of β -pinene (black), α -pinene (blue), limonene (red), isoprene (purple), and
 329 naphthalene (pink) as a function of SOA concentrations in the aqueous phase. The formation
 330 efficiency of OH (molar concentration ratio of OH to SOA: $[\text{BMPO-OH}]/[\text{SOA}]$, in %) in iron
 331 containing SOA water extracts against molar concentration ratios of FeSO_4 and SOA ($[\text{Fe}^{2+}]/[\text{SOA}]$)
 332 by (b) β -pinene, (c) α -pinene, and (d) limonene. The markers are experimental data and the solid
 333 curves with shaded area are modelled with uncertainty.

334

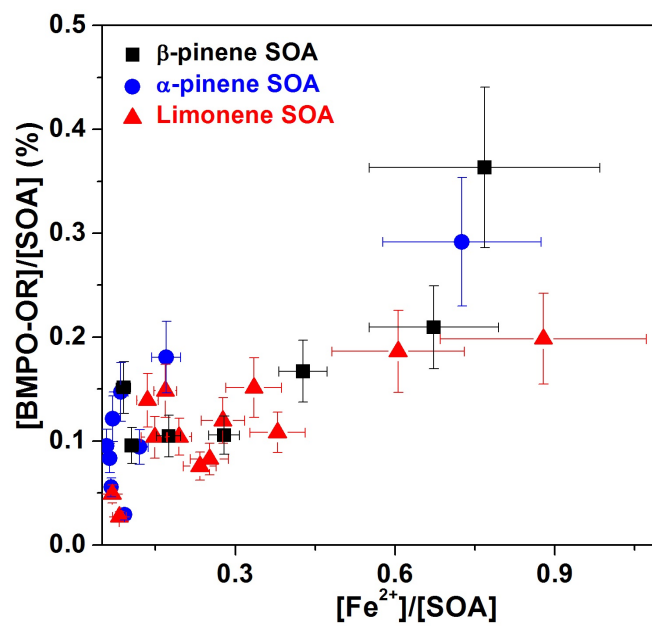


335

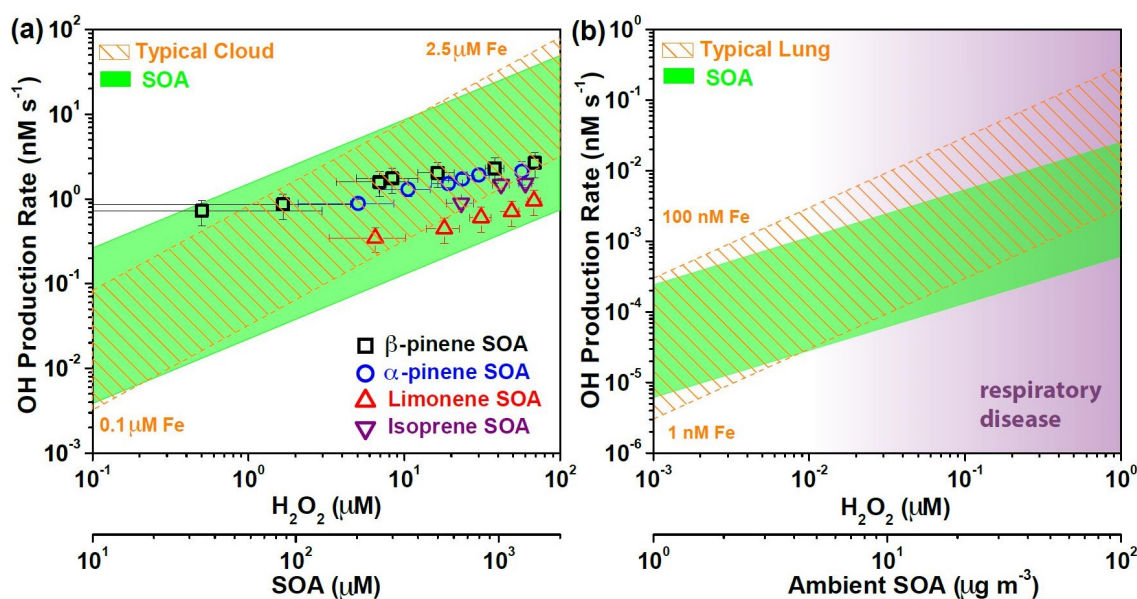
336 **Figure 5. OH yield of β -pinene SOA in three different kinds of pure water: Milli-Q (squares),**
 337 **Savillex (triangles), and TraceSELECT (Sigma, crosses).**

338

339



340
 341 **Figure 6. Formation efficiency of organic radicals.** Molar concentration ratio of organic radicals to
 342 SOA ([BMPO-OR]/[SOA], in %) in mixtures of Fe²⁺ and SOA solutions.
 343

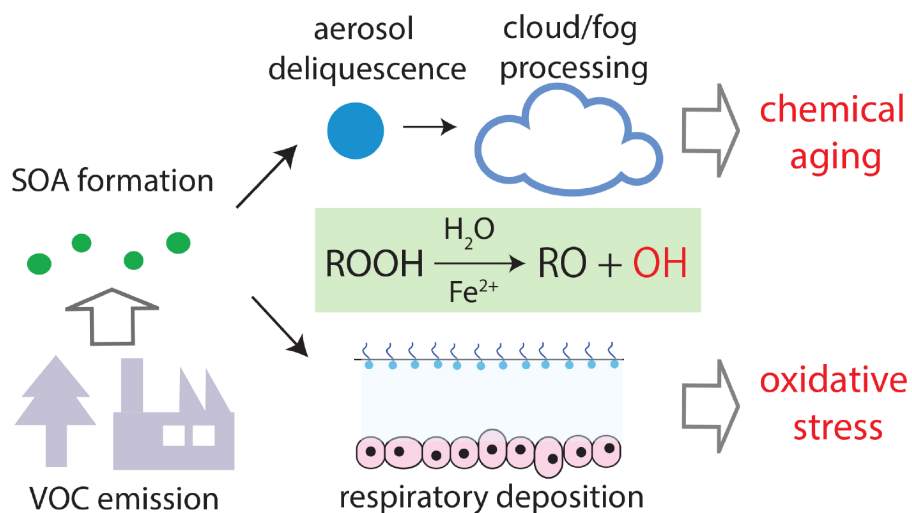


345

346 **Figure 7. OH production rate in cloud droplets and lung lining fluid.** (a) The OH production rate
 347 in cloud droplets by SOA decomposition compared to the classical Fenton reaction. The data points
 348 were measured in the absence of Fe²⁺ for different precursors of β-pinene (black squares), α-pinene
 349 (blue circles), limonene (red upward triangles), and isoprene (purple downward triangles). The shaded
 350 green area represents the possible range in the presence of iron as a function of SOA concentration in
 351 the aqueous phase, which is based on the minimum and maximum OH radical production efficiency
 352 of SOA in Figure 4. The dashed lines represent OH production rates due to the Fenton reaction from
 353 H₂O₂ with typical dissolved iron concentrations (Fe²⁺:Fe³⁺ = 1:1) of 0.1 and 2.5 μM. (b) The OH
 354 production rate in lung lining fluid by SOA decomposition as a function of ambient SOA
 355 concentrations, and by the classical Fenton reaction as a function of H₂O₂ concentrations with typical
 356 dissolved iron concentrations (Fe²⁺: Fe³⁺ = 1:1) of 100 and 1 nM. The purple shaded area represents
 357 patients with respiratory disease exhibiting high H₂O₂ concentrations in the bronchoalveolar
 358 lavage(Corradi et al., 2008).

359

360



361

362 **Figure 8. Implications of OH formation by SOA.** Formation of OH radicals upon decomposition of
 363 organic hydroperoxides (ROOH) in secondary organic aerosol leads to rapid chemical aging of SOA
 364 particles upon deliquescence and cloud or fog processing in the atmosphere as well as oxidative stress
 365 upon inhalation and deposition in the human respiratory tract. Mixing and Fenton-like reactions of
 366 iron with ROOH from SOA can occur both in atmospheric particles and in the lung lining fluid.

367

368 **Acknowledgements.** This work was funded by the Max Planck Society.

369

370 **References.**

371 Anglada, J. M., Martins-Costa, M., Ruiz-López, M. F., and Francisco, J. S.: Spectroscopic signatures
372 of ozone at the air–water interface and photochemistry implications, *Proc. Natl. Acad. Sci. U.S.A.*,
373 111, 11618-11623, 2014.

374 Arakaki, T., Anastasio, C., Kuroki, Y., Nakajima, H., Okada, K., Kotani, Y., Handa, D., Azechi, S.,
375 Kimura, T., and Tshako, A.: A general scavenging rate constant for reaction of hydroxyl radical with
376 organic carbon in atmospheric waters, *Environ. Sci. Technol.*, 47, 8196-8203, 2013.

377 Arangio, A. M., Slade, J. H., Berkemeier, T., Pöschl, U., Knopf, D. A., and Shiraiwa, M.: Multiphase
378 Chemical Kinetics of OH Radical Uptake by Molecular Organic Markers of Biomass Burning
379 Aerosols: Humidity and Temperature Dependence, Surface Reaction, and Bulk Diffusion, *J. Phys.*
380 *Chem. A*, 119, 4533–4544, 2015.

381 Badali, K., Zhou, S., Aljawhary, D., Antiñolo, M., Chen, W., Lok, A., Mungall, E., Wong, J., Zhao,
382 R., and Abbatt, J.: Formation of hydroxyl radicals from photolysis of secondary organic aerosol
383 material, *Atmos. Chem. Phys.*, 15, 7831-7840, 2015.

384 Berkemeier, T., Huisman, A. J., Ammann, M., Shiraiwa, M., Koop, T., and Pöschl, U.: Kinetic
385 regimes and limiting cases of gas uptake and heterogeneous reactions in atmospheric aerosols and
386 clouds: a general classification scheme, *Atmos. Chem. Phys.*, 13, 6663-6686, 2013.

387 Bruns, E. A., El Haddad, I., Keller, A., Klein, F., Kumar, N. K., Pieber, S. M., Corbin, J. C., Slowik, J.
388 G., Brune, W. H., Baltensperger, U., and Prévôt, A. S. H.: Inter-comparison of laboratory smog
389 chamber and flow reactor systems on organic aerosol yield and composition, *Atmos. Meas. Tech.*, 8,
390 2315-2332, 2015.

391 Chen, X., and Hopke, P.: A chamber study of secondary organic aerosol formation by limonene
392 ozonolysis, *Indoor air*, 20, 320-328, 2010.

393 Chen, X., Hopke, P. K., and Carter, W. P.: Secondary organic aerosol from ozonolysis of biogenic
394 volatile organic compounds: chamber studies of particle and reactive oxygen species formation,
395 *Environ. Sci. Technol.*, 45, 276-282, 2010.

396 Chen, X., Hopke, P. K., and Carter, W. P. L.: Secondary Organic Aerosol from Ozonolysis of
397 Biogenic Volatile Organic Compounds: Chamber Studies of Particle and Reactive Oxygen Species
398 Formation, *Environ. Sci. Technol.*, 45, 276-282, 2011.

399 Chu, B., Liu, Y., Li, J., Takekawa, H., Liggio, J., Li, S.-M., Jiang, J., Hao, J., and He, H.: Decreasing
400 effect and mechanism of FeSO₄ seed particles on secondary organic aerosol in α -pinene
401 photooxidation, *Environ. Pollut.*, 193, 88-93, 2014.

402 Corradi, M., Pignatti, P., Brunetti, G., Goldoni, M., Caglieri, A., Nava, S., Moscato, G., and Balbi, B.:
403 Comparison between exhaled and bronchoalveolar lavage levels of hydrogen peroxide in patients with
404 diffuse interstitial lung diseases, *Acta Biomed*, 79, 73-78, 2008.

405 Crounse, J. D., Nielsen, L. B., Jørgensen, S., Kjaergaard, H. G., and Wennberg, P. O.: Autoxidation of
406 organic compounds in the atmosphere, *J. Phys. Chem. Lett.*, 4, 3513-3520, 2013.

407 Deguillaume, L., Leriche, M., Desboeufs, K., Mailhot, G., George, C., and Chaumerliac, N.:
408 Transition Metals in Atmospheric Liquid Phases: Sources, Reactivity, and Sensitive Parameters,
409 Chem. Rev., 105, 3388-3431, 2005.

410 Docherty, K. S., Wu, W., Lim, Y. B., and Ziemann, P. J.: Contributions of organic peroxides to
411 secondary aerosol formed from reactions of monoterpenes with O₃, Environ. Sci. Technol., 39, 4049-
412 4059, 2005.

413 Donahue, N. M., Henry, K. M., Mentel, T. F., Kiendler-Scharr, A., Spindler, C., Bohn, B., Brauers, T.,
414 Dorn, H. P., Fuchs, H., Tillmann, R., Wahner, A., Saathoff, H., Naumann, K.-H., Möhler, O., Leisner,
415 T., Müller, L., Reinnig, M.-C., Hoffmann, T., Salo, K., Hallquist, M., Frosch, M., Bilde, M., Tritscher,
416 T., Barmet, P., Praplan, A. P., DeCarlo, P. F., Dommen, J., Prévôt, A. S. H., and Baltensperger, U.:
417 Aging of biogenic secondary organic aerosol via gas-phase OH radical reactions, Proc. Natl. Acad.
418 Sci. U.S.A., 109, 13503-13508, 2012.

419 Ehn, M., Thornton, J. A., Kleist, E., Sipila, M., Junninen, H., Pullinen, I., Springer, M., Rubach, F.,
420 Tillmann, R., Lee, B., Lopez-Hilfiker, F., Andres, S., Acir, I.-H., Rissanen, M., Jokinen, T.,
421 Schobesberger, S., Kangasluoma, J., Kontkanen, J., Nieminen, T., Kurten, T., Nielsen, L. B.,
422 Jorgensen, S., Kjaergaard, H. G., Canagaratna, M., Dal Maso, M., Berndt, T., Petaja, T., Wahner, A.,
423 Kerminen, V.-M., Kulmala, M., Worsnop, D. R., Wildt, J., and Mentel, T. F.: A large source of low-
424 volatility secondary organic aerosol, Nature, 506, 476-479, 2014.

425 Epstein, S. A., Blair, S. L., and Nizkorodov, S. A.: Direct photolysis of α -pinene ozonolysis secondary
426 organic aerosol: effect on particle mass and peroxide content, Environ. Sci. Technol., 48, 11251-
427 11258, 2014.

428 Ervens, B., Turpin, B., and Weber, R.: Secondary organic aerosol formation in cloud droplets and
429 aqueous particles (aqSOA): a review of laboratory, field and model studies, Atmos. Chem. Phys., 11,
430 11069-11102, 2011.

431 Ervens, B.: Modeling the Processing of Aerosol and Trace Gases in Clouds and Fogs, Chem. Rev.,
432 2015.

433 Faber, P., Drewnick, F., Veres, P. R., Williams, J., and Borrmann, S.: Anthropogenic sources of
434 aerosol particles in a football stadium: Real-time characterization of emissions from cigarette smoking,
435 cooking, hand flares, and color smoke bombs by high-resolution aerosol mass spectrometry, Atmos.
436 Environ., 77, 1043-1051, 2013.

437 Foster, T. L., and Caradonna, J. P.: Fe²⁺-catalyzed heterolytic RO-OH bond cleavage and substrate
438 oxidation: A functional synthetic non-heme iron monooxygenase system, J. Am. Chem. Soc., 125,
439 3678-3679, 2003.

440 Fuller, S., Wragg, F., Nutter, J., and Kalberer, M.: Comparison of on-line and off-line methods to
441 quantify reactive oxygen species (ROS) in atmospheric aerosols, Atmos. Environ., 92, 97-103, 2014.

442 Gehling, W., and Dellinger, B.: Environmentally Persistent Free Radicals and Their Lifetimes in
443 PM_{2.5}, Environ. Sci. Technol., 47, 8172-8178, 2013.

444 Goldstein, S., and Meyerstein, D.: Comments on the mechanism of the "Fenton-like" reaction, Acc.
445 Chem. Res., 32, 547-550, 1999.

446 Gutteridge, J. M. C., Mumby, S., Quinlan, G. J., Chung, K. F., and Evans, T. W.: Pro-oxidant iron is
447 present in human pulmonary epithelial lining fluid: implications for oxidative stress in the lung,
448 Biochem. Biophys. Res. Commun., 220, 1024-1027, 1996.

449 Hallquist, M., Wenger, J. C., Baltensperger, U., Rudich, Y., Simpson, D., Claeys, M., Dommen, J.,
450 Donahue, N. M., George, C., Goldstein, A. H., Hamilton, J. F., Herrmann, H., Hoffmann, T., Iinuma,
451 Y., Jang, M., Jenkin, M. E., Jimenez, J. L., Kiendler-Scharr, A., Maenhaut, W., McFiggans, G.,
452 Mentel, T. F., Monod, A., Prevot, A. S. H., Seinfeld, J. H., Surratt, J. D., Szmigielski, R., and Wildt, J.:
453 The formation, properties and impact of secondary organic aerosol: current and emerging issues,
454 *Atmos. Chem. Phys.*, 9, 5155-5235, 2009.

455 Harris, E., Sinha, B., van Pinxteren, D., Tilgner, A., Fomba, K. W., Schneider, J., Roth, A., Gnauk, T.,
456 Fahlbusch, B., Mertes, S., Lee, T., Collett, J., Foley, S., Borrmann, S., Hoppe, P., and Herrmann, H.:
457 Enhanced Role of Transition Metal Ion Catalysis During In-Cloud Oxidation of SO₂, *Science*, 340,
458 727-730, 2013.

459 Hellpointner, E., and Gäb, S.: Detection of methyl, hydroxymethyl and hydroxyethyl hydroperoxides
460 in air and precipitation, *Nature*, 337, 631-634, 1989.

461 Herrmann, H., Tilgner, A., Barzagli, P., Majdik, Z., Gligorovski, S., Poulain, L., and Monod, A.:
462 Towards a more detailed description of tropospheric aqueous phase organic chemistry: CAPRAM 3.0,
463 *Atmos. Environ.*, 39, 4351-4363, 2005.

464 Huang, R.-J., Zhang, Y., Bozzetti, C., Ho, K.-F., Cao, J.-J., Han, Y., Daellenbach, K. R., Slowik, J. G.,
465 Platt, S. M., Canonaco, F., Zotter, P., Wolf, R., Pieber, S. M., Bruns, E. A., Crippa, M., Ciarelli, G.,
466 Piazzalunga, A., Schwikowski, M., Abbaszade, G., Schnelle-Kreis, J., Zimmermann, R., An, Z.,
467 Szidat, S., Baltensperger, U., Haddad, I. E., and Prevot, A. S. H.: High secondary aerosol contribution
468 to particulate pollution during haze events in China, *Nature*, 514, 218-222, 2014.

469 Jacob, D. J.: Chemistry of OH in remote clouds and its role in the production of formic acid and
470 peroxymonosulfate, *J. Geophys. Res. Atmos.*, 91, 9807-9826, 1986.

471 Jimenez, J. L., Canagaratna, M. R., Donahue, N. M., Prevot, A. S. H., Zhang, Q., Kroll, J. H.,
472 DeCarlo, P. F., Allan, J. D., Coe, H., Ng, N. L., Aiken, A. C., Docherty, K. S., Ulbrich, I. M.,
473 Grieshop, A. P., Robinson, A. L., Duplissy, J., Smith, J. D., Wilson, K. R., Lanz, V. A., Hueglin, C.,
474 Sun, Y. L., Tian, J., Laaksonen, A., Raatikainen, T., Rautiainen, J., Vaattovaara, P., Ehn, M., Kulmala,
475 M., Tomlinson, J. M., Collins, D. R., Cubison, M. J., Dunlea, E. J., Huffman, J. A., Onasch, T. B.,
476 Alfarra, M. R., Williams, P. I., Bower, K., Kondo, Y., Schneider, J., Drewnick, F., Borrmann, S.,
477 Weimer, S., Demerjian, K., Salcedo, D., Cottrell, L., Griffin, R., Takami, A., Miyoshi, T.,
478 Hatakeyama, S., Shimono, A., Sun, J. Y., Zhang, Y. M., Dzepina, K., Kimmel, J. R., Sueper, D.,
479 Jayne, J. T., Herndon, S. C., Trimborn, A. M., Williams, L. R., Wood, E. C., Middlebrook, A. M.,
480 Kolb, C. E., Baltensperger, U., and Worsnop, D. R.: Evolution of organic aerosols in the atmosphere,
481 *Science*, 326, 1525-1529, 2009.

482 Jokinen, T., Berndt, T., Makkonen, R., Kerminen, V.-M., Junninen, H., Paasonen, P., Stratmann, F.,
483 Herrmann, H., Guenther, A. B., Worsnop, D. R., Kulmala, M., Ehn, M., and Sipilä, M.: Production of
484 extremely low volatile organic compounds from biogenic emissions: Measured yields and
485 atmospheric implications, *Proc. Natl. Acad. Sci. U.S.A.*, 112, 7123-7128, 2015.

486 Kalberer, M., Paulsen, D., Sax, M., Steinbacher, M., Dommen, J., Prevot, A., Fisseha, R.,
487 Weingartner, E., Frankevich, V., and Zenobi, R.: Identification of polymers as major components of
488 atmospheric organic aerosols, *Science*, 303, 1659-1662, 2004.

489 Kanakidou, M., Seinfeld, J. H., Pandis, S. N., Barnes, I., Dentener, F. J., Facchini, M. C., Van
490 Dingenen, R., Ervens, B., Nenes, A., Nielsen, C. J., Swietlicki, E., Putaud, J. P., Balkanski, Y., Fuzzi,
491 S., Horth, J., Moortgat, G. K., Winterhalter, R., Myhre, C. E. L., Tsigaridis, K., Vignati, E., Stephanou,
492 E. G., and Wilson, J.: Organic aerosol and global climate modelling: a review, *Atmos. Chem. Phys.*, 5,
493 1053-1123, 2005.

- 494 Kang, E., Root, M., Toohey, D., and Brune, W.: Introducing the concept of potential aerosol mass
495 (PAM), *Atmos. Chem. Phys.*, 7, 5727-5744, 2007.
- 496 Kautzman, K. E., Surratt, J. D., Chan, M. N., Chan, A. W. H., Hersey, S. P., Chhabra, P. S., Dalleska,
497 N. F., Wennberg, P. O., Flagan, R. C., and Seinfeld, J. H.: Chemical Composition of Gas- and
498 Aerosol-Phase Products from the Photooxidation of Naphthalene, *J. Phys. Chem. A*, 114, 913-934,
499 2010.
- 500 Kidd, C., Perraud, V., Wingen, L. M., and Finlayson-Pitts, B. J.: Integrating phase and composition of
501 secondary organic aerosol from the ozonolysis of alpha-pinene, *Proc. Natl. Acad. Sci. U.S.A.*, 111,
502 7552-7557, 2014.
- 503 Koop, T., Bookhold, J., Shiraiwa, M., and Pöschl, U.: Glass transition and phase state of organic
504 compounds: dependency on molecular properties and implications for secondary organic aerosols in
505 the atmosphere, *Phys. Chem. Chem. Phys.*, 13, 19238-19255, 2011.
- 506 Lambe, A. T., Ahern, A. T., Williams, L. R., Slowik, J. G., Wong, J. P. S., Abbatt, J. P. D., Brune, W.
507 H., Ng, N. L., Wright, J. P., Croasdale, D. R., Worsnop, D. R., Davidovits, P., and Onasch, T. B.:
508 Characterization of aerosol photooxidation flow reactors: heterogeneous oxidation, secondary organic
509 aerosol formation and cloud condensation nuclei activity measurements, *Atmos. Meas. Tech.*, 4, 445-
510 461, 2011.
- 511 Lambe, A. T., Chhabra, P. S., Onasch, T. B., Brune, W. H., Hunter, J. F., Kroll, J. H., Cummings, M.
512 J., Brogan, J. F., Parmar, Y., Worsnop, D. R., Kolb, C. E., and Davidovits, P.: Effect of oxidant
513 concentration, exposure time, and seed particles on secondary organic aerosol chemical composition
514 and yield, *Atmos. Chem. Phys.*, 15, 3063-3075, 2015.
- 515 Lim, Y., Tan, Y., Perri, M., Seitzinger, S., and Turpin, B.: Aqueous chemistry and its role in
516 secondary organic aerosol (SOA) formation, *Atmos. Chem. Phys.*, 10, 10521-10539, 2010.
- 517 Lim, Y., and Turpin, B.: Laboratory evidence of organic peroxide and peroxyhemiacetal formation in
518 the aqueous phase and implications for aqueous OH, *Atmos. Chem. Phys.*, 15, 12867-12877, 2015.
- 519 Liu, Y., Monod, A., Tritscher, T., Praplan, A., DeCarlo, P., Temime-Roussel, B., Quivet, E.,
520 Marchand, N., Dommen, J., and Baltensperger, U.: Aqueous phase processing of secondary organic
521 aerosol from isoprene photooxidation, *Atmos. Chem. Phys.*, 12, 5879-5895, 2012.
- 522 McNeill, V. F.: Aqueous organic chemistry in the atmosphere: Sources and chemical processing of
523 organic aerosols, *Environ. Sci. Technol.*, 49, 1237-1244, 2015.
- 524 Mentel, T. F., Springer, M., Ehn, M., Kleist, E., Pullinen, I., Kurtén, T., Rissanen, M., Wahner, A.,
525 and Wildt, J.: Formation of highly oxidized multifunctional compounds: autoxidation of peroxy
526 radicals formed in the ozonolysis of alkenes – deduced from structure–product relationships, *Atmos.*
527 *Chem. Phys.*, 15, 6745-6765, 2015.
- 528 Nam, W., Han, H. J., Oh, S.-Y., Lee, Y. J., Choi, M.-H., Han, S.-Y., Kim, C., Woo, S. K., and Shin,
529 W.: New insights into the mechanisms of OO bond cleavage of hydrogen peroxide and tert-alkyl
530 hydroperoxides by iron (III) porphyrin complexes, *J. Am. Chem. Soc.*, 122, 8677-8684, 2000.
- 531 Ortega, A. M., Hayes, P. L., Peng, Z., Palm, B. B., Hu, W., Day, D. A., Li, R., Cubison, M. J., Brune,
532 W. H., Graus, M., Warneke, C., Gilman, J. B., Kuster, W. C., de Gouw, J. A., and Jimenez, J. L.:
533 Real-time measurements of secondary organic aerosol formation and aging from ambient air in an
534 oxidation flow reactor in the Los Angeles area, *Atmos. Chem. Phys. Discuss.*, 15, 21907-21958, 2015.

- 535 Pavlovic, J., and Hopke, P. K.: Detection of radical species formed by the ozonolysis of α -pinene, *J.*
536 *Atmos. Chem.*, 66, 137-155, 2010.
- 537 Pöhlker, C., Wiedemann, K. T., Sinha, B., Shiraiwa, M., Gunthe, S. S., Smith, M., Su, H., Artaxo, P.,
538 Chen, Q., Cheng, Y., Elbert, W., Gilles, M. K., Kilcoyne, A. L. D., Moffet, R. C., Weigand, M.,
539 Martin, S. T., Pöschl, U., and Andreae, M. O.: Biogenic potassium salt particles as seeds for
540 secondary organic aerosol in the Amazon, *Science*, 337, 1075-1078, 2012.
- 541 Pöschl, U., Martin, S. T., Sinha, B., Chen, Q., Gunthe, S. S., Huffman, J. A., Borrmann, S., Farmer, D.
542 K., Garland, R. M., Helas, G., Jimenez, J. L., King, S. M., Manzi, A., Mikhailov, E., Pauliquevis, T.,
543 Petters, M. D., Prenni, A. J., Roldin, P., Rose, D., Schneider, J., Su, H., Zorn, S. R., Artaxo, P., and
544 Andreae, M. O.: Rainforest Aerosols as Biogenic Nuclei of Clouds and Precipitation in the Amazon,
545 *Science*, 329, 1513-1516, 2010.
- 546 Pöschl, U., and Shiraiwa, M.: Multiphase Chemistry at the Atmosphere–Biosphere Interface
547 Influencing Climate and Public Health in the Anthropocene, *Chem. Rev.*, 115, 4440–4475, 2015.
- 548 Renbaum-Wolff, L., Grayson, J. W., Bateman, A. P., Kuwata, K., Sellier, M., Murray, B. J., Schilling,
549 J. E., Martin, S. T., and Bertram, A. K.: Viscosity of α -pinene secondary organic material and
550 implications for particle growth and reactivity, *Proc. Natl. Acad. Sci. U.S.A.*, 110, 8014-8019, 2013.
- 551 Shiraiwa, M., Ammann, M., Koop, T., and Pöschl, U.: Gas uptake and chemical aging of semisolid
552 organic aerosol particles, *Proc. Natl. Acad. Sci. U.S.A.*, 108, 11003-11008, 2011a.
- 553 Shiraiwa, M., Sosedova, Y., Rouvière, A., Yang, H., Zhang, Y., Abbatt, J. P., Ammann, M., and
554 Pöschl, U.: The role of long-lived reactive oxygen intermediates in the reaction of ozone with aerosol
555 particles, *Nat. Chem.*, 3, 291-295, 2011b.
- 556 Shiraiwa, M., Yee, L. D., Schilling, K. A., Loza, C. L., Craven, J. S., Zuend, A., Ziemann, P. J., and
557 Seinfeld, J. H.: Size distribution dynamics reveal particle-phase chemistry in organic aerosol
558 formation, *Proc. Natl. Acad. Sci. U.S.A.*, 110, 11746-11750, 2013.
- 559 Solomon, S.: *Climate change 2007-the physical science basis: Working group I contribution to the*
560 *fourth assessment report of the IPCC*, Cambridge University Press, Cambridge, 2007.
- 561 Stoll, S., and Schweiger, A.: EasySpin, a comprehensive software package for spectral simulation and
562 analysis in EPR, *J. Magn. Reson.*, 178, 42-55, 2006.
- 563 Truong, H., Lomnicki, S., and Dellinger, B.: Potential for misidentification of environmentally
564 persistent free radicals as molecular pollutants in particulate matter, *Environ. Sci. Technol.*, 44, 1933-
565 1939, 2010.
- 566 Venkatachari, P., and Hopke, P. K.: Development and evaluation of a particle-bound reactive oxygen
567 species generator, *J. Aerosol. Sci.*, 39, 168-174, 2008.
- 568 Virtanen, A., Joutsensaari, J., Koop, T., Kannosto, J., YliPirilä, P., Leskinen, J., Mäkelä, J. M.,
569 Holopainen, J. K., Pöschl, U., Kulmala, M., Worsnop, D. R., and Laaksonen, A.: An amorphous solid
570 state of biogenic secondary organic aerosol particles, *Nature*, 467, 824-827, 2010.
- 571 Wang, Y., Kim, H., and Paulson, S. E.: Hydrogen peroxide generation from alpha- and beta-pinene
572 and toluene secondary organic aerosols, *Atmos. Environ.*, 45, 3149-3156, 2011.
- 573 Waring, M. S.: Secondary organic aerosol in residences: predicting its fraction of fine particle mass
574 and determinants of formation strength, *Indoor Air*, 24, 376-389, 2014.

- 575 Weber, R. T.: Xenon Data Processing Reference 2012.
- 576 Weschler, C. J.: Chemistry in indoor environments: 20 years of research, *Indoor Air*, 21, 205-218,
577 2011.
- 578 Yamazaki, I., and Piette, L. H.: ESR spin-trapping studies on the reaction of Fe^{2+} ions with H_2O_2 -
579 reactive species in oxygen toxicity in biology, *J. Biol. Chem.*, 265, 13589-13594, 1990.
- 580 Zhao, H., Joseph, J., Zhang, H., Karoui, H., and Kalyanaraman, B.: Synthesis and biochemical
581 applications of a solid cyclic nitron spin trap: a relatively superior trap for detecting superoxide
582 anions and glutathyl radicals, *Free Radic. Biol. Med.*, 31, 599-606, 2001.
- 583 Zhu, B.-Z., Shan, G.-Q., Huang, C.-H., Kalyanaraman, B., Mao, L., and Du, Y.-G.: Metal-
584 independent decomposition of hydroperoxides by halogenated quinones: Detection and identification
585 of a quinone ketoxy radical, *Proc. Natl. Acad. Sci. U.S.A.*, 106, 11466-11471, 2009.
- 586
- 587